Computational Materials Science 150 (2018) 244–251

Contents lists available at ScienceDirect

Computational Materials Science

journal homepage: www.elsevier.com/locate/commatsci

Modelling of austenite transformation along arbitrary cooling paths

Aarne Pohjonen*, Mahesh Somani, David Porter

University of Oulu, Materials and Production Technology, Pentti Kaiteran Katu 1, 90014 Oulu, Finland

ARTICLE INFO

Keywords:
Phase transformations
Bainite
Martensite
Thermomechanical processing
Steel

ABSTRACT

A computational model based on the Johnson-Mehl-Avrami-Kolmogorov equation for simulating the onset and kinetics of austenite to bainite and martensite transformation has been fitted to experimental continuous cooling data for two different steels. We investigated how deformation below recrystallization temperature affected the transformation onset and kinetics in comparison to the same steel in the undeformed state. The fitted model can be used to simulate phase transformations occurring when the steel is cooled along any cooling path. The model can be fully coupled to heat transfer and conduction simulations in order to optimize cooling practice, for example in industrial thermomechanical processing of steel. The fitted model can also be used to predict the hardness of the steel after cooling.

1. Introduction

In order to be able to control the final mechanical properties of hot-rolled steels, it is important to understand how prior deformation below the no-recrystallization temperature and subsequent fast cooling affect the transformation of austenite into bainite and martensite, as well as how the different phase fractions affect the mechanical properties of the steel. Since the deformation affects the subsequent transformations during cooling, a model which can be fitted to describe the effects is needed. There exist a large number of computational models, which can be used to calculate the austenite decomposition during cooling. Two main types of kinetics models are frequently used, namely the Kirkaldy-Venugopalan model, e.g. [1–4] and the Johnson-Mehl-Avrami-Kolmogorov (JMAK) type model, e.g. [5–12].

In this study, fresh attempts have been made to computationally simulate the effect of deformation on phase transformation by calculating the transformation onset for an arbitrary cooling path and fitting the widely used JMAK equation and Koistinen-Marburger type equation [13] to a discrete sets of experimental data to describe the kinetics after the onset. To calculate transformation onset for an arbitrary cooling path, a method described in Refs. [14–19] is used. For cooling paths leading to mixtures of bainite and martensite, we need to be able to model the case when not all of the austenite is transformed into bainite. Therefore we use the differential form of the JMAK equation [7,8] which includes description for the maximum fraction of bainite that can be transformed at different temperatures. We apply the functional form for the rate parameter obtained from comparison to experimental bainite transformation rate [20]. The aim of the present model is that it can be used in predicting the onset and kinetics of phase transformations and also the hardness of the steel, when it is cooled along any linear or nonlinear cooling path. The model has been fitted to data for two different steels which were either in the undeformed (i.e. recrystallized) or deformed condition, i.e. 0.6 compressively strained below the no-recrystallization temperature Tnr.

The aim of this article is to describe the applied computational method. In the current article the model parameters have been fitted to each case separately. If the presented model is fitted to a large number of different experimental cases, it can be used to investigate systematically how the parameters are affected by the deformation. However, since the exact parameter dependence on deformation conditions and/or steel chemistry, precipitation of the alloying elements etc. requires dedicated experimental programs, this will be the focus of future studies, while the current article provides the computational and theoretical framework that can be used in such studies.

Once the model has been fitted for the corresponding deformation conditions, it is useful in controlling the final mechanical properties of hot-rolled steel by enabling the design of an optimized cooling path commensurate with the actual direct quenching practice. Since the model has been fitted for two steels subjected to two different conditions (deformed below recrystallization temperature vs. undeformed), we can see how the exact deformation condition described here affects the transformation rate for the steels. In addition, since the more detailed microstructure models have to produce correct macroscopic transformation behavior, the fitted model parameters provide information on the possible ranges of parameters in more detailed microstructure models, such as a cellular automata model.

* Corresponding author.
E-mail address: Aarne.Pohjonen@Oulu.fi (A. Pohjonen).

https://doi.org/10.1016/j.commatsci.2018.03.052
Received 19 October 2017; Received in revised form 2 March 2018; Accepted 23 March 2018
Available online 20 April 2018

Table 1
Chemical compositions (wt.%) of the experimental steels along with their M_S [21] and Tnr [22] temperatures.

Steel	C	Si	Mn	Al	Cr	Mo	Ti	Nb	Ni	V	Cu	B	M_S	Tnr
1	0.20	0.34	0.72	0.06	1.00	0.48	0.033	0.002	1.01	0.004	0.013	0.0029	412	881
2	0.20	0.34	1.48	0.06	0.24	0.01	0.031	0.032	1.01	0.004	0.011	0.0028	401	987

2. Materials and experimental

2.1. Compositions of experimental steels

The chemical compositions of the two boron-bearing 0.2 C steels selected for this study are given in Table 1. While Steel 1 has been alloyed with about 1% Cr, 0.48% Mo and relatively lower Mn (0.72%), Steel 2 is microalloyed with 0.032% Nb and has a higher level of Mn (1.48%) and less Cr (0.24%). Both steels were microalloyed with approximately 30 ppm boron, which was protected from reaction with nitrogen (about 40 ppm) by the addition of ≈0.03% Ti, while Si (0.34%) and Ni (1%) were maintained at the same levels for both the steels. Impurity elements like S and P were controlled to below 50 ppm for both the steels.

The steels were cast as 70 kg slabs (500 × 300 × 55 mm) at Outokumpu Stainless Oyj, Tornio, Finland. They were subsequently homogenized and hot rolled at the University of Oulu to 12 mm thick plates. Also included in Table 1 are the martensite start temperature (M_S) [21] (pp. 82–126), and the no-recrystallization temperature (Tnr) [22].

2.2. Dilatation measurements

CCT diagrams were determined with the aid of dilatation measurements using a Gleeble 1500 thermomechanical simulator. Cylindrical specimens of dimensions 6 mm dia × 9 mm were machined from solution treated and water quenched laboratory rolled samples. Two types of dilatation tests were made: with or without prior strain. In the case of straining, samples were heated at 20 °C/s to 1100 °C, held for 4 min, cooled to 850 °C, held 10 s, and then compressed with three hits each having a strain of ~0.2 at a strain rate of 1/s. The time between hits was 25 s. The specimens were then held 25 s before cooling at various linear rates in the range 1.5–48 °C/s, Fig. 1. For comparison, another set of specimens was reheated in a similar manner, cooled at 2 °C/s to 1000 °C and held for 2 min prior to cooling. These two sets of simulation experiments are meant to simulate water cooling (quenching) after hot rolling with high finish rolling temperatures and after controlled rolling finishing at low temperatures below Tnr.

Vickers hardness measurements were carried out on all the specimens using a 5 kg load. Dilatation curves were supplemented in some cases with light optical examinations of the final microstructures. This allowed the presence of small quantities of polygonal ferrite to be ascertained when ferrite formation was not clear on the basis of the dilatation curves alone.

Analysis of dilatation curves showing percent change in diameter vs. temperature was carried out both for unstrained and 3x0.2 strained austenite. Austenite decomposition into ferrite, bainite, martensite or a mixture of these phases can be ascertained by the inflexions in the dilatation curves, as described elsewhere [23]. CCT diagrams were plotted from the dilatation data to delineate the effect of cooling rate and prior strain on the phase transformation characteristics, as revealed by the dilatation curves.

3. Calculations

Our objective is to construct a model, which can be parameterized using experimental dilatometry data, and can give an estimate for the austenite to bainite and/or martensite transformations for *any* cooling path, as well as an estimate for the hardness of the steel after cooling. The model is based on well known phenomenological equations [5,12,13,20], and it is parameterized using continuous cooling data.

3.1. Calculation of transformation onset and kinetics for any cooling path

The volume fraction χ of bainite transformed from austenite during time t at a given temperature can be calculated with the JMAK equation [12], which includes the transformation start time, Eq. (1)

$$\chi = [1-exp(-[k(t-t_{1\%})]^n)]\chi_{max} \quad (1)$$

where $t_{1\%}$ is the start time required for 1% transformation of bainite, which includes the incubation time. The function k and exponent n have to be determined by fitting to experimental data. χ_{max} is the maximum volume fraction that can be transformed, which can be 100% in the temperature regime where martensite does not form. While the parameter n is assumed to be constant, k depends on temperature T, as described later.

To calculate an estimate for the start of the transformation and the subsequent transformation kinetics for any cooling path, the cooling path is divided into small isothermal segments and the transformation start time is calculated by applying the Scheil's additivity rule and the so-called ideal TTT in a similar way as in [15,16,18]. The main idea of

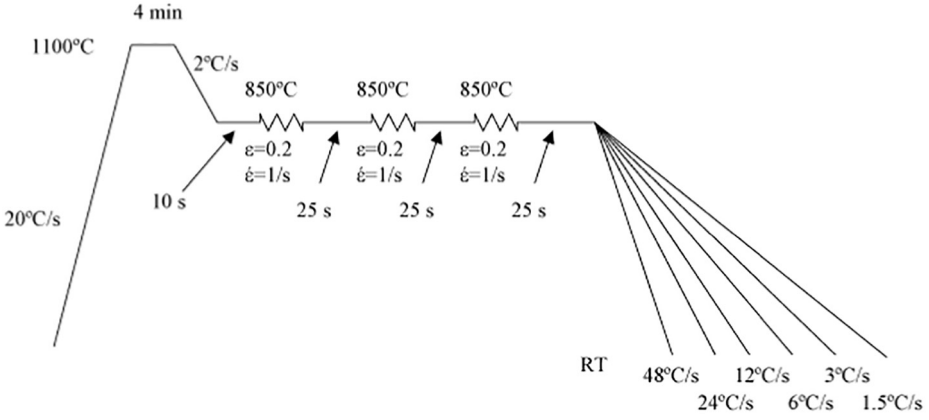

Fig. 1. Simulated dilatation experiments to construct the CCT diagrams – tests after 3 × 0.2 prior strain.

the method is briefly described here. The ideal TTT is the TTT diagram which produces exactly the correct CCT transformation start for constant cooling rates. To construct the ideal TTT diagram, a smooth curve is fitted to the 1% transformed CCT curve. A functional form of $t_{85}(T) = c\exp(a\exp(bT))$, where t_{85} is the time spent between 800 °C and 500 °C and a,b,c constants, provided a good fit for interpolation of the experimental data from the CCT diagram where t_{85} is plotted on the x-axis and 1% transformation temperatures T_{cct} are plotted on the y-axis. Then, the experimentally obtained CCT diagram is transformed to the ideal TTT diagram using Eq. (2) [15,16,14,24]

$$\frac{1}{t_{1\%}(T)} = -\frac{d\dot{\theta}(T_{cct})}{dT_{cct}} \tag{2}$$

where $\dot{\theta}(T_{cct}) = 300/t_{85}$ is the constant cooling rate which results in 1% transformation at temperature T_{cct}. To be able to extrapolate the calculation of $t_{1\%}(T)$ outside of the fitting range of the CCT diagram, the functional form described by Eq. (3) was used.

$$t_{1\%}(T) = K_{1\%}(B_{S1\%}-T)^{-m_{1\%}}\exp\left(\frac{Q_{1\%}}{R(T+273.15)}\right) \tag{3}$$

where the parameters $K_{1\%}$,$B_{S1\%}$,$m_{1\%}$, and $Q_{1\%}$ are obtained from least squares fitting to the $t_{1\%}(T)$ curve using the Matlab function "lsqfit". The effect of changing chemical composition can be estimated from the results presented in [17].

After the conversion of the CCT curve to the ideal TTT curve, the transformation start can be calculated for any cooling path using the ideal TTT diagram and Scheil's additivity rule, i.e. the cooling curve is divided into small isothermal timesteps $\Delta t(T)$ and the estimate for 1% transformation is calculated when the sum in Eq. (4) equals unity.

$$\sum \frac{\Delta t(T)}{t_{1\%}(T)} = 1 \tag{4}$$

Once the transformation start has been reached, the following model is used to calculate the transformation kinetics (i.e. when $\chi > 1\%$). An expression for the transformation rate can be obtained by solving $t-t_{1\%}$ and $\exp(-[k(t-t_{1\%})]^n)$ from Eq. (1) and substituting them to the time derivative of Eq. (1), $d\chi/dt$, which yields Eq. (5) [8,9].

$$\frac{d\chi}{dt} = (\chi_{max}-\chi)\left[ln\left(\frac{\chi_{max}}{\chi_{max}-\chi}\right)\right]^{\frac{n-1}{n}} nk(T) \tag{5}$$

Once the temperature dependent function $k(T)$ and the Avrami exponent n are known, the amount of bainite formed, $\Delta\chi$, during timestep Δt can be calculated as $\Delta\chi = \frac{d\chi}{dt}\Delta t$. For this purpose we now seek for the correct functional form for $k(T)$.

Based on the analysis of a large number of isothermal experiments [20], the growth rate of bainite from austenite can be described by the phenomenological Eq. (6).

$$\frac{d\chi}{dt} = A(\chi)(B_S-T)^p exp\left(\frac{-Q}{R(T+273.15)}\right) \tag{6}$$

where $A(\chi)$ is a function of the fraction transformed, B_S is the limiting temperature for bainite formation and p and Q are constant parameters, which are obtained by fitting the model to experimental results. Comparing Eqs. (5) and (6), it can be seen that because only $k(T)$ depends on temperature, it is justified to use the functional form given by Eq. (7) for the temperature dependence of $k(T)$.

$$k(T) = K(B_S-T)^p exp\left(\frac{-Q}{R(T+273.15)}\right) \tag{7}$$

where K is a fitting constant. Since $k(T)^n$ is the product of the nucleation and growth rates, it should be proportional to the number of available nucleation sites. If the fraction of austenite transformed into martensite is χ_m, the maximum fraction of bainite, which can form is the remaining austenite fraction, $\chi_{max} = 1-\chi_m$.

For the martensite transformation, the Koistinen-Marburger type equation, Eq. (8), was used

$$\chi_m = [1-exp(-k_m(M_S-T))](1-\chi_b) \tag{8}$$

where k_m and the martensite start temperature M_S are fitting parameters, and χ_b is the bainite fraction.

The transformation kinetic model parameters, n,K,Q,p,k_m and M_S were fitted using the Nelder-Mead algorithm with the MatLab fminsearch function [25], which minimised the total difference between experimental and computed value of the temperatures, where 5%, 25%, 50%, 75% and 95% austenite volume fraction were transformed at different cooling rates. For steel 1, B_S was computed using the equation given in [26], but for steel 2, it was necessary to fit the value of B_S, since the value given by the same equation was too low, when compared to the experimental results. The comparison between the fitted model and experimental data is shown in Fig. 4.

3.2. Calculation of hardness after cooling along any cooling path

We wish to calculate an estimate for the hardness of the steel after cooling along any path. If all austenite is transformed to bainite and martensite $\chi_b + \chi_m = 1$. Since the hardness is mostly determined by the fractions of bainite and martensite, we assume that the total hardness H_{tot} can be calculated by the rule of mixtures, $H_{tot} = \chi_b H_b + \chi_m H_m$, where H_b and H_m are the hardness of bainite and martensite. Since cooling rate has an appreciable effect on the bainite hardness due to the possibility of the formation of the of both upper and lower bainite or a mixture of the two depending on the cooling rate, we consider this effect in similar way as in [6,27], using the functional form of $H_b = C + A\log(V)$, where C and A are constants and V is the cooling rate. Using these relations, the total hardness H_{tot} can be calculated from the fractions of bainite and martensite and the applied cooling rate using Eq. (9).

$$\chi_b(C + A\log(V)) + \chi_m H_m = H_{\text{tot}} \tag{9}$$

According to [27] A can be calculated from the chemical composition from the steel: $A = 89 + 53C-55Si-22Mn-10Ni-20Cr-33Mo$, where the symbols for the elements represent their mass percentage in the steel. The constant C is fitted, as described below. Assuming there is no retained austenite at room temperature, Eq. (9) can be rewritten in the form of Eq. (10)

$$C + \frac{\chi_m}{1-\chi_m}H_m = \frac{H_{\text{tot}}}{1-\chi_m} - A\log(V) \tag{10}$$

where H_{tot} is measured from the constant cooling rate experiments, χ_m is obtained from the calculations for different cooling rates and A is obtained from the composition. The values for C and H_m can then be obtained from the linear fit, using Eq. (10), by plotting $(1-\chi_m)/\chi_m$ on the x-axis and the right hand side of Eq. (10) on the y-axis. Once the values of H_m and C are determined, the hardness can be estimated for any cooling path based on the phase transformation calculations and application of Eq. (9) by using an average cooling rate for the temperature regime where bainite is formed.

4. Results and discussion

The comparison between the computed and experimental values for the transformation onset (i.e. 1% transformed) are shown in Fig. 2 for constant cooling rates. The ideal TTT diagrams, which were obtained using Eqs. (2) and (3) are shown in Fig. 3. Applying Scheil's additivity rule, Eq. (4), and the ideal TTT diagram, Eq. (3), the transformation onset can be calculated for any cooling path. For both steels, the prior deformation in the no recrystallization regime shifted the transformation onset curve to longer times and lower temperatures. For steel 2 it seems that the higher temperature part of the CCT and ideal TTT onset diagrams was not much affected by the deformation, but the lower

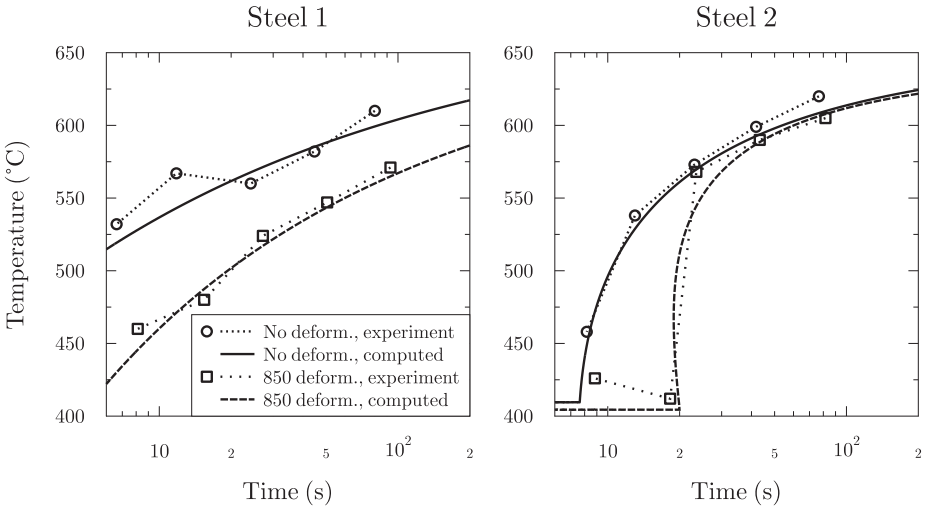

Fig. 2. Comparison between experimental and calculated transformation start during continuous cooling. Each marker corresponds to an experimental cooling rate and the lines represent the results calculated using Eq. (4). The experimental cooling rates were 48, 24, 12, 6, and 3 °C/s.

temperature part was shifted towards longer times. The transformation onset parameters for the steels and deformation conditions are given in Table 2. For the steel 1, the CCT nose was not visible in the experimental data. For this reason, the values for $Q_{1\%}$ were estimated based on a previous analysis [18] and literature data [28]. The model reproduces the experimental data well, as shown in Fig. 2, which is sufficient for cases where cooling rates are restricted to the range used in the experiments. For steel 2, the CCT nose is visible in the experiments, and in this case the parameters also give realistic extrapolation to faster and slower cooling rates. For all cases the experimental onset data is reproduced reasonably well by our model.

The model parameters were fitted to the experimental data for the undeformed steel as well as for the steel subjected to 3 × 0.2 strain at 850 °C. The parameters obtained from the fitting are shown in Table 3.

The bainite and martensite fractions which form during cooling along any cooling path can be calculated with Eqs. (1) and (7) using the parameter values presented in Table 3. The comparison between the computed and experimental values for the transformation kinetics is shown in Fig. 4.

It is well known that the austenite grain size affects the austenite decomposition. Different authors have included this effect by scaling factors, which effectively scale the magnitude of the transformation rate according to the grain size [1,6,10,29]. The deformation of austenite below the recrystallization temperature may, however, affect the transformation kinetics in more complex ways than simply scaling the rate of transformation. The introduction of slip bands as well as dislocation cell structures create new nucleation sites with lowered

Table 2
The onset model parameters obtained from fitting.

Steel	Strain	$K_{1\%}$	$B_{S1\%}$ (°C)	$Q_{1\%}$ (kJ/mol)	$m_{1\%}$
Steel 1	No strain	$1.7{\cdot}10^{7}$	715	74	5.7
Steel 1	0.6 at 850 °C	$2.0{\cdot}10^{6}$	677	35	3.7
Steel 2	No strain	0.45	652	60	1.5
Steel 2	0.6 at 850 °C	$2.4{\cdot}10^{-4}$	640	98	0.90

Table 3
The kinetic model parameters.

Steel	Strain	K	n	$Q\left(\frac{\text{kJ}}{\text{mol}}\right)$	p	B_S (°C)	k_m	M_S (°C)
Steel 1	No strain	1.00	0.67	89.92	1.600	564	−0.0244	413.9
Steel 1	0.6 at 850 °C	2.02	1.70	38.97	0.756	564	−0.0242	414.4
Steel 2	No strain	0.976	1.61	60.66	1.375	652	−0.0241	400.0
Steel 2	0.6 at 850 °C	0.620	1.19	60.42	1.250	652	−0.0210	404.9

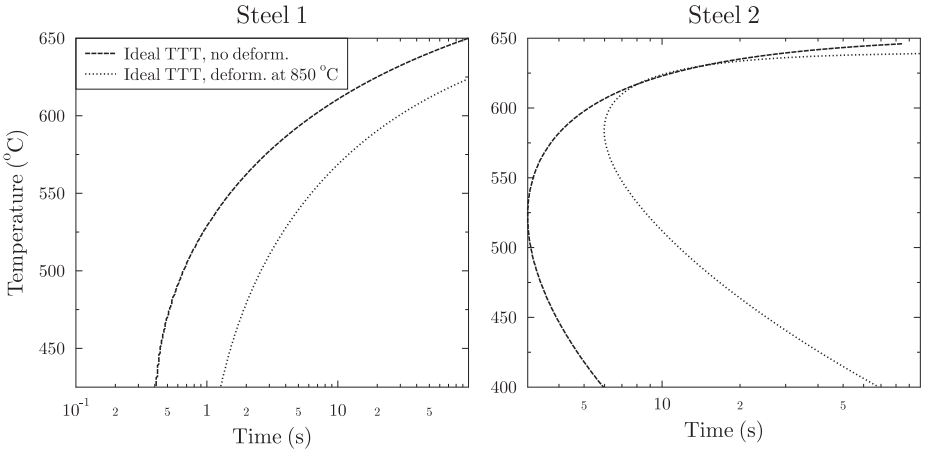

Fig. 3. The ideal TTT diagram representing $t_{1\%}(T)$, which was calculated using Eq. (2) from constant cooling rate experiments. The ideal TTT diagram is applied in the calculation of the transformation start for any cooling path applying the Scheil's additivity rule, Eq. (4).

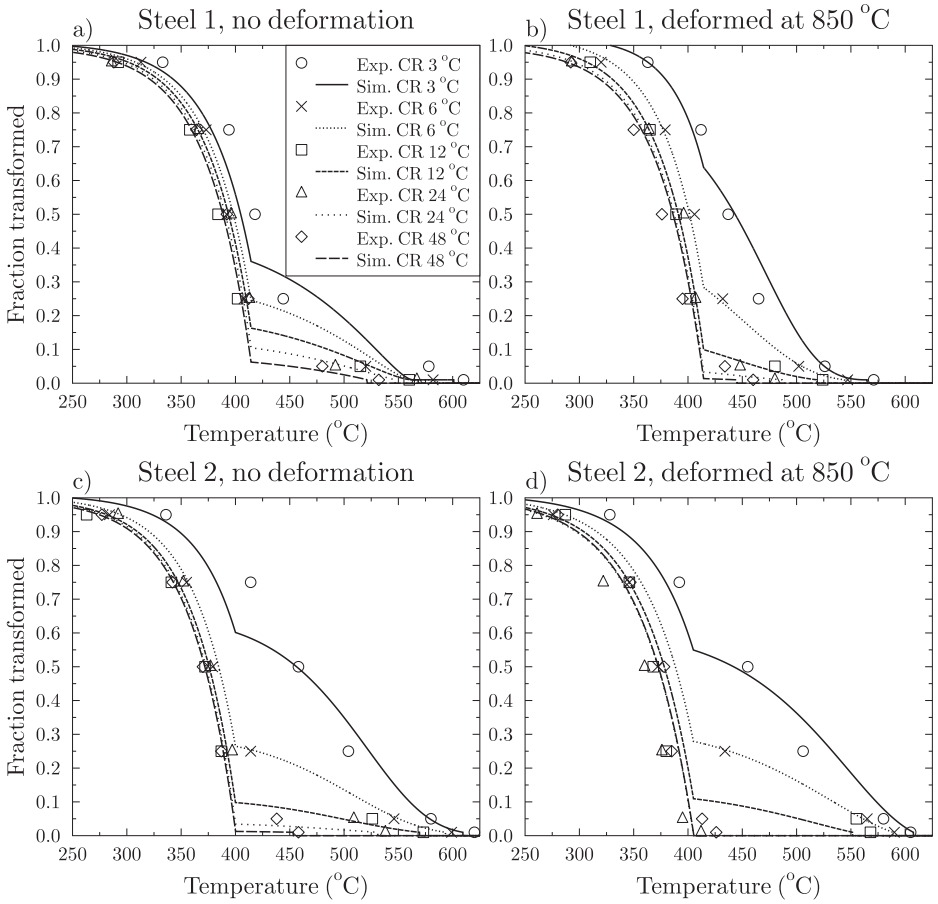

Fig. 4. The fraction transformed for different cooling rates. Simulated results (lines) compared with the experimental results (markers).

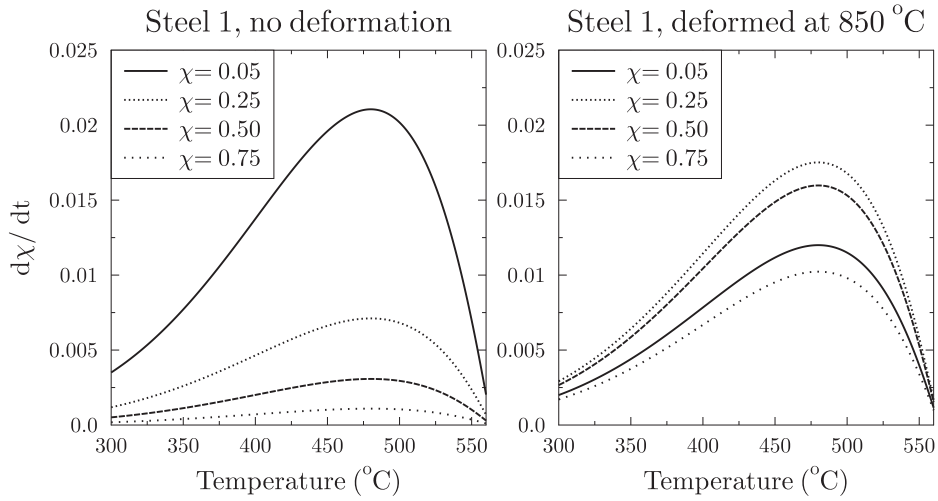

Fig. 5. Calculated transformation rate of bainite for steel 1. The transformation rate $d\chi/dt$ depends on temperature T and the fraction of bainite which has been formed, χ, according to Eq. (5).

activation energy and the pancaked austenite may slow the transformation process by introducing barriers to the growth of bainite and martensite. These effects are inherently included in the model when the parameters are fitted. Although the straining has been included in other transformation models by scaling the rate as function of strain, as described in reference [10], the exact functional form describing the transformation rate dependence on straining is currently unknown. Accurate determination of transformation rate dependence on straining would require an experimental program, and the model presented in this article can be used as a computational framework for such studies.

The transformation rate of bainite, which depends on temperature and the fraction of bainite formed, is shown in Fig. 5 for both the undeformed and deformed steel 1. For the cooling of undeformed steel 1, the transformation rate is first more rapid for $\chi = 5\%$ bainite formed, but slows down quickly when the transformation proceeds. In contrast, for the deformed steel 1, the transformation rate increases as the transformation proceeds and then slows down. The transformation rate of bainite both for the undeformed and deformed steel 2 is shown in

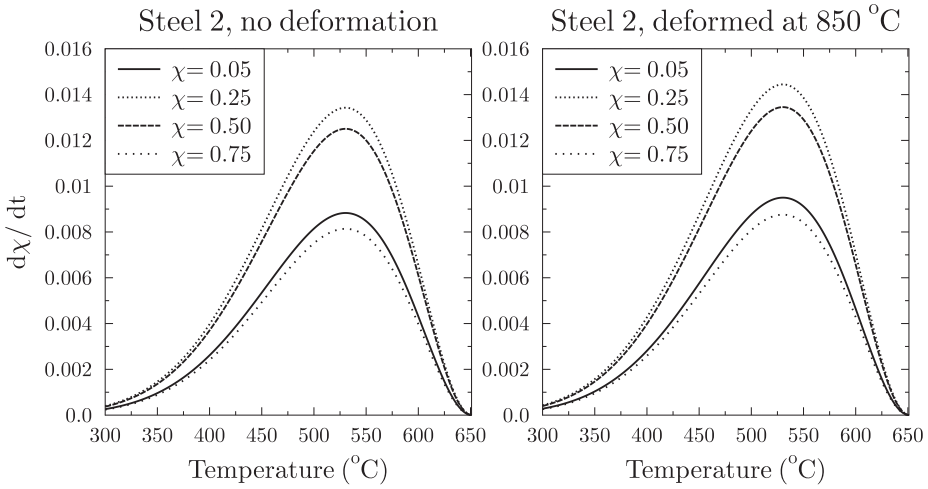

Fig. 6. Calculated transformation rate of bainite for steel 2. The transformation rate $d\chi/dt$ depends on temperature T and the fraction of bainite which has been formed, χ, according to the Eq. (5).

Table 4
The hardness of martensite and the parameters for calculating the hardness of bainite. Using these values and the calculated phase fractions, an estimate for the hardness of the steel can be calculated for a steel cooled along any cooling path, using Eq. (9) and using the average cooling rate during bainite formation as V.

Steel	Strain	H_m	C	A
Steel 1	No strain	476.0	330.0	19.12
Steel 1	0.6 at 850 °C	485.2	356.7	19.12
Steel 2	No strain	451.7	326.5	33.11
Steel 2	0.6 at 850 °C	472.2	291.0	33.11

Fig. 6. For steel 2 the deformation only had a small effect on the transformation kinetics.

The hardness of martensite and the parameters for calculating the hardness of bainite, are shown in Table 4. Using these values and the average cooling rate during the formation of bainite, an estimate of the hardness of the cooled steel can be obtained using Eq. (9).

The method allows calculation of bainite and martensite fractions which form during cooling along any cooling path using Eqs. (5) and (7), as well as the calculation of the hardness of the steel after the cooling using Eq. (9). To easily calculate these quantities when the steel is cooled along any cooling path, a simple graphical user interface has been constructed [30], which allows the user to define the cooling path. The fitted phase transformation model has also been fully coupled to heat conduction and transfer simulations, but the results of those simulations are out of the scope of the current article and will be published later elsewhere. The fitted rate parameter function also provides information for the possible range of parameters in more detailed microstructure models, such as for example a cellular automata model [5], since the rate parameter is the product of nucleation and growth rates.

To demonstrate the usage of the model in optimizing cooling path in order to achieve desired amounts of bainite and martensite, and to validate the model for nonlinear cooling paths, we applied our simple graphical user interface (GUI) to design a cooling path which produces desired amount of bainite and martensite [30]. The GUI is shown in Fig. 7. User can select the cooling path by clicking on the canvas, the path is submitted to the phase transformation calculation, and the user receives the result within a second. By trying different cooling paths, the user can find a suitable path which produces desired amount of bainite and martensite.

A validation test was performed following the cooling path designed with the tool shown in Fig. 7. The thermomechanical path with

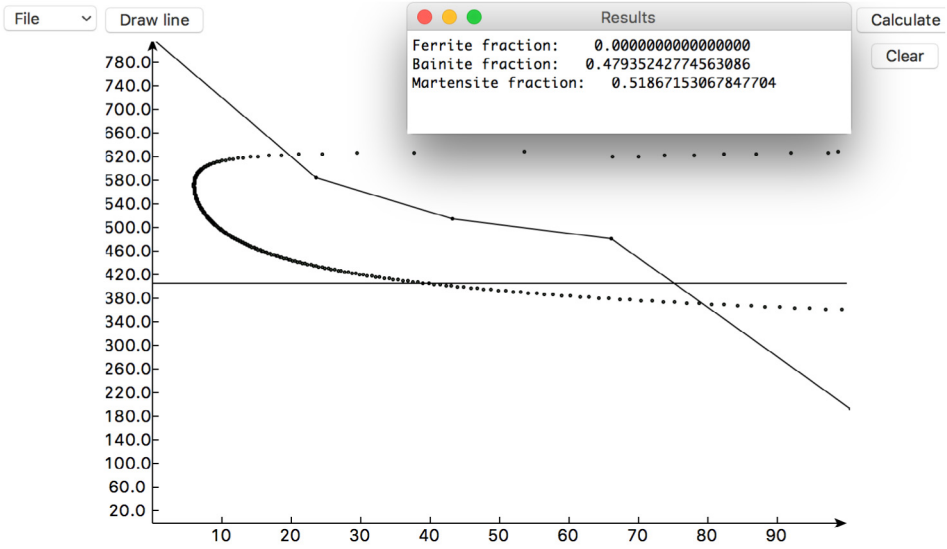

Fig. 7. A graphical user interface has been developed for experimenting with different cooling paths in order to obtain desired amount of bainite and martensite.

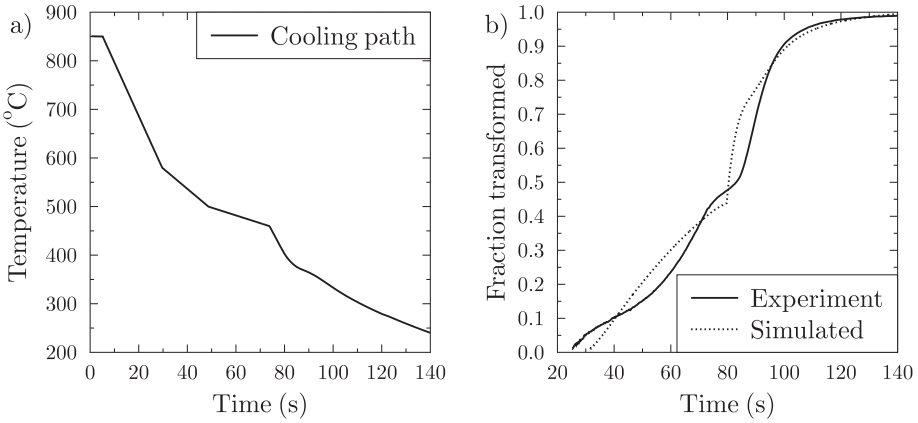

Fig. 8. (a) To validate the computational model, the same nonlinear cooling path as used in the experiment was simulated with the current model. (b) The comparison of the computational model to experimentally observed fraction transformed calculated from dilatometry data as function of time shows reasonably good agreement.

deformation at 850 °C described in Section 2 for steel 2 prior to cooling was used. The corresponding simulation with the fitted parameters was carried out. The actual measured cooling path, shown in Fig. 8a), was used in the simulation. The transformed fraction calculated from the experimental measurements is compared to the simulated transformed fraction as function of time in Fig. 8b). The comparison shows that the simulation reproduces the experimentally observed transformation behavior with reasonably good accuracy.

5. Conclusions

Model which can be used in calculating the phase transformation onset and kinetics, when a steel is cooled along any cooling path has been applied to describe two steels subjected to two deformation conditions. When experimental CCT dilatometry data and microscopy estimation of final fractions of transformation products is available, the model can be fitted to the data in order to study how different phenomena in thermomechanical processing affects the model parameters. The model can be used in optimizing desired amounts of bainite and martensite. The model can also be fully coupled with heat conduction simulations in order to estimate phase transformations in objects which have non-uniform temperature distributions during cooling. Thinking of future work concerning detailed microstructure models, the fitted model together with microscopy provides information on the range of values the parameters in such models can have.

6. Data availability

The raw/processed data required to reproduce these findings cannot be shared at this time due to technical or time limitations. The processed data required to reproduce these findings are available to download through the home page of the first author of this article www.iki.fi/aarne.pohjonen.

Acknowledgements

The work described in this paper was made as a part of a research and development programme known as System Integrated Metals Processing (SIMP) which was coordinated by DIMECC Oy (Digital, Internet, Materials and Engineering Co-Creation). The financial support of the Finnish Funding Agency for Technology(Tekes) is gratefully acknowledged.

References

[1] J.S. Kirkaldy, D. Venugopalan, Prediction of microstructure and hardenability in low alloy steels, Int. Conf. Phase Transform. Ferrous Alloys (1983) 125–148.
[2] D. Martin, Selected Heat Conduction Problems in Thermomechanical Treatment of Steel, Juvenes Print, Tampere, Finland, 2011.
[3] D. Watt, L. Coon, M. Bibby, J. Goldak, C. Henwood, An algorithm for modeling microstructural development in weld heat-affected zones. A. Reaction-kinetics, Acta Metall. 36 (11) (1988) 3029–3035, http://dx.doi.org/10.1016/0001-6160(88)90185-X.
[4] N. Saunders, Z. Guo, X. Li, A. Miodownik, J. P. Schillé, The calculation of ttt and cct diagrams for general steels, JMatPro Software Literature.
[5] L. Rauch, R. Kuziak, M. Pietrzyk, From high accuracy to high efficiency in simulations of processing of dual-phase steels, Metall. Mater. Trans. B 45 (2) (2014) 497–506, http://dx.doi.org/10.1007/s11663-013-9926-5.
[6] X. Chen, N. Xiao, D. Li, G. Li, G. Sun, The finite element analysis of austenite decomposition during continuous cooling in 22MnB5 steel, Model. Simul. Mater. Sci. Eng. vol. 22, 6.http://dx.doi.org/10.1088/0965-0393/22/6/065005.
[7] J. Leblond, J. Devaux, A new kinetic-model for anisothermal metallurgical transformations in steels including effect of austenite grain-size, Acta Metall. 32 (1) (1984) 137–146, http://dx.doi.org/10.1016/0001-6160(84)90211-6.
[8] J. Leblond, G. Mottet, J. Devaux, D. JC, Mathematical models of anisothermal phase transformations in steels, and predicted plastic behavior, Mater. Sci. Technol. 1 (10) (1985) 815–822.
[9] R.Pandi, M. Militzer, E. Hawbolt, T. Meadowcroft, Modelling of austenite decomposition kinetics in steels during run-out table cooling, in: E. B. Hawbolt, S. Yue (Eds.), Proceedings of the International Symposium on Phase Transformations During the Thermal/Mechanical Processing of Steel, 1995, pp. 459–471.
[10] S. Serajzadeh, Prediction of temperature distribution and phase transformation on the run-out table in the process of hot strip rolling, Appl. Math. Model. 27 (11) (2003) 861–875, http://dx.doi.org/10.1016/S0307-904X(03)00085-4.
[11] F. Fernandes, S. Denis, A. Simon, Mathematical model coupling phase transformation and temperature evolution during quenching of steels, Mater. Sci. Technol. 1 (10) (1985) 838–844.
[12] M. Avrami, Kinetics of phase change. 2. Transformation time relations for random distribution of nuclei, J. Chem. Phys. 8 (2) (1940) 212–224, http://dx.doi.org/10.1063/1.1750631.
[13] D. Koistinen, R. Marburger, A general equation prescribing the extent of the austenite-martensite transformation in pure iron-carbon alloys and plain carbon steels, Acta Metall. 7 (1) (1959) 59–60, http://dx.doi.org/10.1016/0001-61(59)90170-1 http://www.sciencedirect.com/science/article/pii/0001616059901701 .
[14] J. Kirkaldy, R. Sharma, A new phenomenology for IT and CCT curves, Scripta Metall. 16 (10) (1982) 1193–1198, http://dx.doi.org/10.1016/0036-9748(82)90095-3.
[15] T. Pham, E. Hawbolt, J. Brimacombe, Predicting the onset of transformation under noncontinuous cooling conditions 1. Theory, Metall. Mater. Trans. A – Phys. Metall. Mater. Sci. 26 (8) (1995) 1987–1992, http://dx.doi.org/10.1007/BF02670670.
[16] T. Pham, E. Hawbolt, J. Brimacombe, Predicting the onset of transformation under noncontinuous cooling conditions: Part 2. Application to the austenite pearlite transformation, Metall. Mater. Trans. A 26 (8) (1995) 1993–2000, http://dx.doi.org/10.1007/BF02670671.
[17] A. Pohjonen, M. Somani, J. Pyykkönen, J. Paananen, D. Porter, The onset of the austenite to bainite phase transformation for different cooling paths and steel compositions, Vol. 716 of Key Engineering Materials, 2016.
[18] A. Pohjonen, A. Kaijalainen, M. Somani, J. Larkiola, Analysis of bainite onset during cooling following prior deformation at different temperatures, Comput. Methods Mater. Sci. 17 (1).
[19] E. Scheil, Anlaufzeit der austenitumwandlung, Arch. Eisenhuttenwes 8 (1935) 565–567.
[20] A. Borgenstam, M. Hillert, Kinetics of bainite transformation in steels, in: E. Pereloma, D.V. Endmonds (Eds.), Phase Transformations in Steels: Fundamentals and Diffusion-Controlled Transformations, Elsevier, 2012, pp. 470–501.
[21] K. Thelning, Steel and its heat treatment, Butterworth, 1975.
[22] F. Boratto, R. Barbosa, S. Yue, J.J. Jonas, Effect of Chemical Composition on the Critical Temperatures of Microalloyed Steels, in: Proc. International Conference on Physical Metallurgy of Thermomechanical Processing of Steels and Other Metals (THERMEC'88), Tokyo, 1988, pp. 383–390.
[23] M.C. Somani, J.M. Pyykkonen, D.A. Porter, L.P. Karjalainen, J.I. Komi, J. Mater. Perform. Charact. 4 (3) (2015) 341–364.
[24] I. Wierszyllowski, The effect of the thermal path to reach isothermal temperature on transformation kinetics, Metall. Trans. A – Phys. Metall. Mater. Sci. 22 (5) (1991)

993–999, http://dx.doi.org/10.1007/BF02661092.
[25] Matlab documentation, <https://se.mathworks.com/help/matlab/>, (accessed: 25.8.2017).
[26] W. Steven, A. G. Haynes, The temperature of formation of martensite and bainite in low-alloy steels.
[27] P. Maynier, J. Dollet, P. Bastien, Hardenability concepts with applications to steels, 1978, pp. 518–44.
[28] M. Kang, M.-X. Zhang, F. Liu, M. Zhu, Kinetics and morphology of isothermal transformations at intermediate temperature in 15CrMnMoV Steel, Mater. Trans. 50 (1) (2009) 123–129, http://dx.doi.org/10.2320/matertrans.MRA2008194.
[29] M. Militzer, E. Hawbolt, T. Meadowcroft, Microstructural model for hot strip rolling of high-strength low-alloy steels, Metall. Mater. Trans. A – Phys. Metall. Mater. Sci. 31 (4) (2000) 1247–1259, http://dx.doi.org/10.1007/s11661-000-0120-4.
[30] A. Pohjonen, V. Kyllönen, J. Paananen, Analytical Approximations and Simulation Tools for Water Cooling of Hot Rolled Steel Strip, in: Proceedings of the 9th EUROSIM Congress on Modelling and Simulation, Linköping University Conference Proceedings, in press.